

Journal of Materials Chemistry C

Accepted Manuscript



This is an *Accepted Manuscript*, which has been through the Royal Society of Chemistry peer review process and has been accepted for publication.

Accepted Manuscripts are published online shortly after acceptance, before technical editing, formatting and proof reading. Using this free service, authors can make their results available to the community, in citable form, before we publish the edited article. We will replace this *Accepted Manuscript* with the edited and formatted *Advance Article* as soon as it is available.

You can find more information about *Accepted Manuscripts* in the [Information for Authors](#).

Please note that technical editing may introduce minor changes to the text and/or graphics, which may alter content. The journal's standard [Terms & Conditions](#) and the [Ethical guidelines](#) still apply. In no event shall the Royal Society of Chemistry be held responsible for any errors or omissions in this *Accepted Manuscript* or any consequences arising from the use of any information it contains.



Journal Name

ARTICLE

Triggering DRAM/SRAM memory behaviors by single atom substitution to alter molecular planarity

Haiyan Hu, Jinghui He, Hao Zhuang, Erbo Shi, Hua Li*, Najun Li, Dongyun Chen, Qingfeng Xu, Jianmei Lu*, Lihua Wang

Received 00th January 20xx,
Accepted 00th January 20xx

DOI: 10.1039/x0xx00000x

www.rsc.org/

In this paper, two molecules (E)-6,6'-bis(benzo[b]thiophen-2-yl)-1,1'-bis(2-ethylhexyl)-[3,3'-biindolinylidene]-2,2'-dione (ID(BT)2) and (E)-6,6'-di(benzofuran-2-yl)-1,1'-bis(2-ethylhexyl)-[3,3'-biindolinylidene]-2,2'-dione (ID(BF)2) were designed and synthesized, in which isoindigo acted as the electron acceptor and benzoheterocycles acted as electron donors. The result illustrated that as the heteroatom in the benzoheterocycle was changed from O to S atom, the intramolecular dihedral angle enlarged from 0.3° to 23°. ID(BT)2 based device exhibited SRAM memory characteristic and the ID(BF)2 based device exhibited DRAM behaviour. The enlarged dihedral angle would prolong the process of the excited electrons in the LUMO energy level moving back to the original HOMO energy level, in other words, the ON state of ID(BT)2 based device need more time to return to the original OFF state and thus to exhibit SRAM performance. ID(BF)2 is almost planarity and has less barrier to impede the excited electrons to recovery to the original state, therefore the ID(BF)2 based device could return back to OFF state in a very short time and exhibited DRAM characteristic. This is a new viewpoint of achieving different type of memory device through changing the steric geometry and improving the intramolecular dihedral angle to impede the charge transferability.

Introduction

Organic semiconductor materials have arisen scientific attentions since the last two decades due to their definite structures,¹ easy purification,² large scalability and low cost.³ Thus, they are considered as the potential substitutes to the inorganic materials in the fields of OFET, solar cells, sensors and data storage devices.⁴ After successfully designing and synthesizing series of D-A structural molecules with excellent memory behaviours, our group desire to set up the relationship between the molecular structures and the memory performance through the regulation of different electron donors and acceptors in the backbone,⁵ the molecular conjugated length,⁶ the side soft chain length and the molecular planarity.⁷ These methods have been proved effectively to enhance intermolecular pi-pi stacking and to improve film morphology quality thus to reduce the device power consumption. However, less attention has been paid to tuning of molecular structures to achieve different type of memory device, such as Write-Once-Read-Many Times (WORM), Flash, Static-Random-Access-Memory (SRAM) and

Dynamic-Random-Access-Memory (DRAM) devices. At the beginning of organic and polymeric memory device coming into sight, several excellent researches have been reported by selecting strong or weak electron-acceptor groups into the molecular backbone to achieve different types of data storage devices.⁸ In these reports, the electron-acceptors served as the traps to block the migration the charge carriers. In addition, the stronger the electron-withdraw ability of the acceptor is, the deeper the trap depth will be, which is consistent with the ability of seizing the injected charges. If the electron acceptor is strong enough, it can firmly seize the injected charges and the device would remain in the ON state permanently to show WORM characteristic, while the electron acceptor becomes weaker, their seized charges can be drove out by the reverse electric field or even automatically flee out, which lead to the device exhibit Flash, SRAM or DRAM characteristics. Therefore, these reported literatures have considered that the memory device type is mainly controlled by the electron acceptor in the molecular backbone.

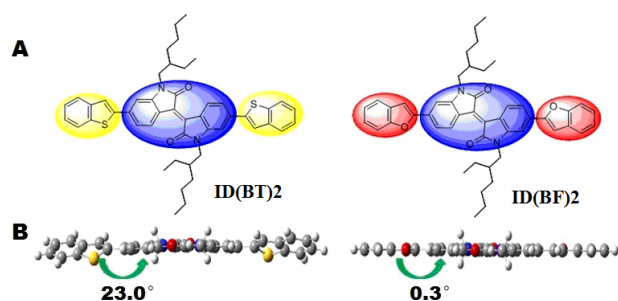
However, the charge trap theory ignored the role of electron donating groups. As we all know, furan received far less attention than thiophene in organic semiconductors due to its earlier examples of instability under oxidative conditions.⁹ However, Nakamura etc have found that benzofuran based small molecules exhibited entirely planarity, dense crystal packing and high hole mobility, all of which are attributed to the small radius of the oxygen atom.¹⁰ Conversely, the radius of sulfur atom is larger than that of oxygen atom, thus, the

College of Chemistry, Chemical Engineering and Materials Science, Collaborative Innovation Center of Suzhou Nano Science and Technology, Soochow University, Suzhou 215123, China. E-mail: lujm@suda.edu.cn
Fax: +86 512 65880367; Tel: +86 512 65880368

†Electronic Supplementary Information (ESI) available: [Thermo gravimetric analysis of the both molecules, the UV-vis spectra of the molecules, the AFM images and NMR spectra of the terminal compound. The I-V switching behaviour of the ITO/molecules/LiF/Al device]. See DOI: 10.1039/x0xx00000x

thiophene derivatives are easy to form intramolecular dihedral angle due to the steric effect.

Isoindigo (ID) can offer strong intramolecular charge transfer and potential possibility for small bandgap donor-acceptor system, and is widely applied as the electron-acceptor in the design of photoelectronic materials.¹¹ Thus, in this paper, we designed and synthesized two molecules, ID(BF)2 and ID(BT)2, with an ID core and two different end-capping electron-donor groups, benzothiophene and benzofuran, respectively, as shown in Scheme 1A. Molecular simulation results illustrate that ID(BF)2 and ID(BT)2 possess different intramolecular dihedral angles, and the memory devices fabricated with them exhibit different type of memory behaviours. This is a new viewpoint of changing electron donors and thus the intramolecular dihedral angle to realize different types of memory devices.



Scheme 1. A) Molecular structures of ID(BF)2 and ID(BT)2; B) optimized geometries of ID(BT)2 and ID(BF)2 backbone units by DFT calculation using the Gaussian 03 with the B3LYP/6-31G

Experimental

Materials

6-bromooxindole, 6-bromoisatin, potassium carbonate, 1-bromo-2-ethylhexane, Potassium carbonate, P(o-tyl)₃, K₃PO₄, Benzothiophene-2-ylboronic acid, Benzofuran-2-ylboronic acid and all the solvents were purchased from Shanghai Chemical Reagent Co. Ltd. All chemicals were used as received without further purification. The two original compounds 3a and 3b were prepared according to previously reported procedures.^{10(a), 11(b)}

Instrumentation and characterizations

NMR spectra were measured on an INOVA 400 MHz spectrometer. Thermo gravimetric analysis (TGA) was conducted on a TA instrument Dynamic TGA 2950 at a heating rate of 10 °C min⁻¹ under a N₂ flow rate of 50 mL min⁻¹. UV-visible absorption spectra were noted on a Perkin-Elmer λ-17 UV-vis spectrometer. Atomic force microscopy (AFM) measurements were performed with MFP-3DTM (Digital Instruments/Asylum Research) AFM instrument in tapping mode. Cyclic Voltammetry (CV) measurements were using a

CHI-660C electrochemical workstation. Scanning electron microscopy (SEM) images were characterized using a Hitachi S-4700 scanning electron microscope. With an X'Pert-Pro MPD X-ray diffractometer, the X-ray diffraction (XRD) patterns were measured. Quantum chemical calculations were performed by using the density functional theory (DFT) with the Gaussian 03 program. The memory devices were carried out with Hewlett-Packard 4145B semiconductor parameter analyzer with a Hewlett-Packard 8110A pulse generator.

Synthesis of the molecules

The synthesis routes of ID(BT)2 and ID(BF)2 are shown in Scheme 2. All of the intermediate and final products are characterized by H-NMR to ensure the correct structure and purity.

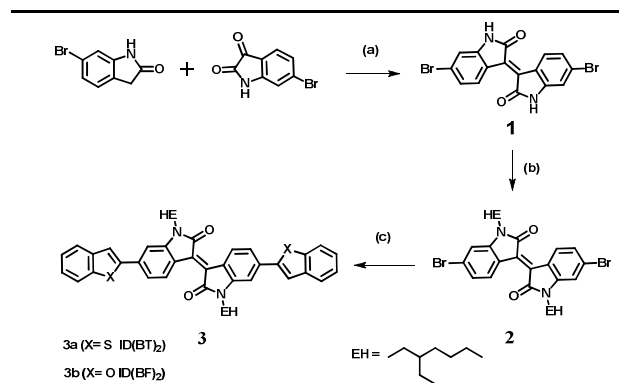
Synthesis of 6, 6'-Dibromoisindigo (1). 6-bromooxindole (500 mg, 2.36 mmol) and 6-bromoisatin (533 mg, 2.36 mmol) were diluted in AcOH (25 mL). Then the conc. HCl solution (0.1 mL) was added into the mixture and the reaction mixture was kept under stirring and reflux for 24 h. After cooling, the mixture was filtered. The solid was successively washed with water, ethyl alcohol and ethyl acetate. After drying under vacuum, 6, 6'-dibromoisindigo was obtained as brown powder (89%). ¹H NMR (400 MHz, DMSO-d₆, ppm): δ: 11.09 (s, 2H), 8.99 (d, J = 8.6 Hz, 2H), 7.18 (d, J = 8.6 Hz, 2H), 6.98 (s, 2H).

Synthesis of 6, 6'-Dibromo-N,N'-(1-octyl)-isoindigo (2). Under nitrogen atmosphere, compound 6, 6'-dibromoisindigo (420 mg, 1.0 mmol) and potassium carbonate (824 mg, 6.0 mmol) were dissolved in DMF (20 mL) and the reaction mixture was stirred for about 30 min. Then 1-bromo-2-ethylhexane (424 mg, 2.2 mmol) was injected, and then the mixture was stirred for 15 h at 100 °C. After the reaction, the mixture was cooled, poured into water and extracted with CH₂Cl₂. The organic layers were washed with brine and water, and then dried with anhydrous MgSO₄. Afterwards, the solvent was removed by rotational evaporation, and the residue was purified by silica chromatography (eluent CH₂Cl₂/PE = 1/2 (v/v), 6,6'-dibromo-N,N'-(2-ethylhexyl)-isoindigo was obtained as red powder (87%). ¹H NMR (400 MHz, CDCl₃, ppm): δ: 9.05 (d, J = 8.5 Hz, 2H), 7.16 (d, J = 8.5 Hz, 2H), 6.90 (s, 2H), 3.65 (d, J = 21.8 Hz, 4H), 1.97 – 1.90 (m, 2H), 1.39 – 1.25 (m, 16H), 1.0 – 0.89 (m, J = 15.2, 7.1 Hz, 12H).

(E)-6,6'-bis(benzo[b]thiophen-2-yl)-1,1'-bis(2-ethylhexyl)-[3,3'-biindolinylidene]-2,2'-dione (3a). Compound 6, 6'-dibromo-N,N'-(2-ethylhexyl)-isoindigo (130 mg, 0.2 mmol), Pd₂(dba)₃ (15 mg), P(o-tyl)₃ (10 mg) and K₃PO₄ (1.2g, 5 mmol) were dissolved in THF (15 mL). The mixture was heated to 40-50 °C under nitrogen atmosphere for 0.5 h. Benzo[b]thiophene-2-ylboronic acid (93 mg, 0.2 mmol) was diluted in THF (10 mL) and the solution was transferred to the mixture through a septum. Then, the mixture was heated to 80 °C and stirred for 12 h. After the reaction, the cooled solution was extracted with CH₂Cl₂. Organic portion was combined and washed with brine and water, and then dried with anhydrous MgSO₄. After removing the solvent by rotational evaporation, the residue was purified by silica chromatography, eluting with (PE/CH₂Cl₂ = 4/1-2/1, v/v). Finally product 3a was obtained as brownish red solid (70%). ¹H NMR (400 MHz, CDCl₃, ppm): δ: 9.21 (d,

$J = 8.4$ Hz, 2H), 7.85 (d, 2H), 7.81 (d, $J = 6.7, 2.0$ Hz, 2H), 7.63 (s, 2H), 7.41 (d, $J = 8.4, 1.7$ Hz, 2H), 7.38–7.33 (m, $J = 11.0, 6.2, 3.6$ Hz, 4H), 7.06 (s, 2H), 3.77–3.67 (m, 4H), 1.93–1.88 (m, 2H), 1.46–1.32 (m, 16H), 0.98 (t, $J = 7.3, 1.5$ Hz, 6H), 0.93 (t, $J = 7.0$ Hz, 6H). m. p. (249.5 °C~251.2 °C).

Compound **3b** was synthesized using a similar procedure as **3a**. (65%). $^1\text{H NMR}$ (400 MHz, CDCl_3 , ppm): δ : 9.23 (d, $J = 8.4$ Hz, 2H), 7.61 (d, $J = 7.4$ Hz, 2H), 7.56–7.53 (m, $J = 13.9, 5.1$ Hz, 4H), 7.33 (t, $J = 7.2$ Hz, 2H), 7.28 (s, 1H), 7.24 (s, 3H), 7.14 (s, 2H), 3.80–3.68 (m, $J = 14.1, 6.7$ Hz, 4H), 1.97–1.97 (m, 2H), 1.45–1.25 (m, 16H), 0.96–0.93 (m, $J = 14.0, 6.0$ Hz, 12H). m. p. (218.5 °C~219.7 °C).



Scheme 2. Synthetic route of the molecule ID(BT)2 and ID(BF)2. (a) Cond HCl (cat.) acetic acid, reflux, >95%. (b) 3-(bromomethyl)heptane, K_2CO_3 , DMF, 100 °C, 85%. (c) benzofuran-2-ylboronic acid or benzo[*b*]thiophen-2-ylboronic acid, N_2 , $\text{Pd}_2(\text{dba})_3$, $\text{P}(\text{o}-\text{tlyl})_3$, K_3PO_4 , THF, 85 °C.

Fabrication and measurements of the ITO/ molecule /Al electrical memory devices.

The ITO glass substrates were pre-cleaned in ultrasonic bath consecutively for 20 min in de-ionized water, acetone and ethanol in turn. The 1, 2-dichloroethane solution of molecule (10 mg/mL) was spin-coated on the ITO glass substrates. Spin parameters: the TIMER A: 100 r/min, 6 s; The TIMER B: 2000 r/min, 30 s. After spin-coating, the films were dried in vacuum overnight. The film thickness was typically about 60 nm. Top aluminium electrodes with thickness of around 100 nm were formed through a mask via thermal evaporation under high vacuum of 2.0×10^{-6} Torr to eventually give the ITO/molecule/Al device with a sandwiched structure.

Results and Discussion

Thermal properties

Thermo gravimetric analysis (TGA) was utilized to explore the thermal stability of the two molecules (Fig. S1). The thermal decomposition temperature of 5% weight loss (T_d) are measured to be 242 °C and 345 °C for ID(BF)2 and ID(BT)2, respectively. The lower T_d of ID(BF)2 can be explained by the clear melting point at 220 °C which is consistent with the melting point of ID(BF)2 between 218.5 °C and 219.7 °C.¹² However, ID(BF)2 can maintain stable below 240 °C, which could basically meet the requirement in future practical applications.

Molecular simulation

To examine the steric geometries of ID(BT)2 and ID(BF)2, density functional theory (DFT) calculations using the Gaussian 03 program based on the B3LYP/6-31G have been performed. In order to simplify the simulation, the alkyl chains are replaced with methyl groups. Scheme 1A is the molecular structures of ID(BT)2 and ID(BF)2 and Scheme 1B shows the theoretical calculated structural optimizations which illustrate an almost planar structure for ID(BF)2 with the intramolecular dihedral angle of 0.3° and a twist structure for ID(BT)2 with that of 23° between the benzoheterocycles and the isoindigo core. The different planarity of the molecules would induce different conjugated planes which may affect the charge transferability in the molecular backbone and would also cause different intermolecular stacking that is a key factor to influence the performance of the semiconductor layers.

Optical and Electrochemical characteristics

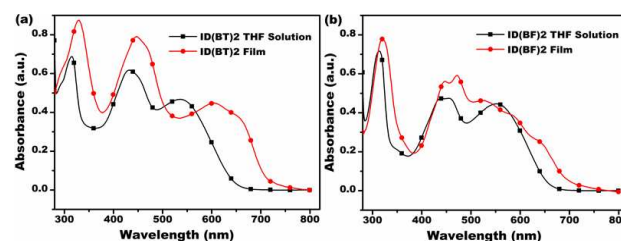


Fig. 1 The UV-vis spectra of ID(BT)2 and ID(BF)2 in THF solution and as thin films. (a) ID(BT)2; (b) ID(BF)2

Fig. S2 shows the UV-vis spectra of ID(BT)2 and ID(BF)2 in THF solution. The absorbance peaks located at 550 nm and 534 nm for ID(BF)2 and ID(BT)2 are consistent with the intramolecular charge transfer (ICT) from the electron-donors to the electron-acceptors.¹³ Compared with ID(BT)2, the CT absorbance peak of ID(BF)2 is red-shifted for about 16 nm, which indicates a stronger CT ability in the molecular backbone. This is mainly arising from the increased pi-conjugation plane due to the almost planar structure. Compared to the UV-vis spectra in solution state, the CT absorption peaks of ID(BT)2 and ID(BF)2 are both prominent red-shifted and significant broadened in film state (Fig. 1). However, the ID(BT)2 film is red-shifted larger than ID(BF)2 film, which is mainly due to the better delocalization of the electrons over the whole molecule when thiophene is used rather than furan. Meanwhile, better delocalization of electrons is advantageous to the intermolecular stacking for ID(BT)2, which is conducive to the formation of molecular aggregation in thin film. Thus, the absorption peak of ID(BT)2 in film state is obvious red-shifted from that of ID(BF)2.¹⁴ Additionally, ID(BF)2 shows a shoulder peak in film state, which indicates an ordered intermolecular stacking due to the planar and rigid conjugated backbone.¹⁵

The electrochemical properties of the two small molecules were investigated by cyclic voltammetry (CV). The onset oxidations ($E_{\text{onset}}^{\text{ox}}$) of these molecules were obtained in anhydrous tetrahydrofuran solution with 0.1 M tetrabutylammonium perchlorate. Ag/AgCl was applied as the reference electrode to measure the electrochemical potentials. The external ferrocene/ferrocenium (Fc/Fc^+) redox standard potential ($E_{\text{ferrocene } 1/2}$) was 0.41 V vs. Ag/AgCl in anhydrous

tetrahydrofuran and the onset oxidations ($E_{\text{onset}}^{\text{ox}}$) of ID(BT)2 and ID(BF)2 were measured to be 1.25 eV and 1.20 eV, respectively (Fig. 2).

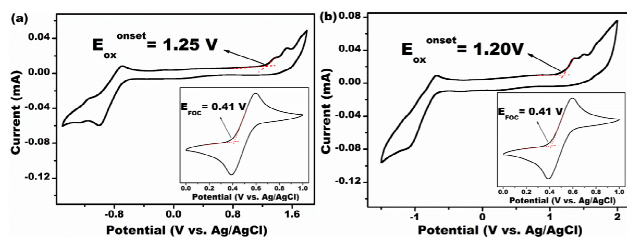


Fig. 2 Cyclic voltammograms of (a) ID(BT)2 and (b) ID(BF)2 on Pt electrode in CH₂Cl₂ solution with 0.1 mol/L Bu₄NPF₆ as supporting electrolyte.

Meantime, the highest occupied molecular orbital (HOMO) energy level of the Fc/Fc⁺ redox standard potential is -4.80 eV with respect to the zero vacuum level. The HOMO and the lowest unoccupied molecular orbital (LUMO) energy levels can be obtained by the

following equations: $E_{\text{HOMO}} = -(E_{\text{onset}}^{\text{ox}} + 4.8 - E_{\text{FOC}})$, $E_{\text{LUMO}} = -(E_{\text{onset}}^{\text{red}} + 4.8 - E_{\text{FOC}})$,¹⁶ and the detailed results are summarized in Table 1. As the work function of ITO is -4.8 eV and that of Al is -4.3 eV, the energy barriers of hole injection from the ITO electrode into the HOMO energy levels of both molecules were estimated to be 0.84 eV for ID(BT)2 and 0.79 eV for ID(BF)2. Furthermore, the energy barriers of electron injection from the Al electrode into the LUMO energy level were estimated to be 0.62 eV for ID(BT)2 and 0.59 eV for ID(BF)2. Thus the electron injection from Al electrode into LUMO energy levels of both molecules are easier than the hole injection from ITO electrode into HOMO energy levels of both molecules (with Al as cathode and ITO as anode), which illustrated that both molecules were n-type materials, and the conduction process is dominated by electrons.¹⁷ It should be noticeable that the electron injection barrier of ID(BT)2 based device is larger than that of ID(BF)2 based device, which would lead to different switching voltages for ID(BT)2 and ID(BF)2 based devices.

Table 1 Optical and electrochemical properties of ID(BT)2 and ID(BF)2.

Molecule	E_{ox} (eV) ^a	E_{red} (eV) ^b	HOMO (eV) ^c	LUMO (eV) ^d	$\Phi_{\text{ITO-HOMO}}$ (eV)	LUMO- Φ_{Al} (eV)
ID(BT)2	1.25	-0.71	-5.64	-3.68	0.84	0.62
ID(BF)2	1.20	-0.68	-5.59	-3.71	0.79	0.59

Potential vs. Ag/AgCl in a 0.1 M anhydrous acetonitrile solution of tetrabutylammonium perchlorate (TBAP). ^aOnset oxidation potential vs. Ag/AgCl. ^bOnset reduction potential vs. Ag/AgCl. ^cThe HOMO energy levels were calculated from cyclic voltammetry with reference to ferrocene (0.41 eV): $\text{HOMO} = -[E_{\text{ox}} + 4.8 - E_{\text{Ferrocene}}^{\text{ox}}]$. ^d $\text{LUMO} = -[E_{\text{red}} + 4.8 - E_{\text{Ferrocene}}^{\text{ox}}]$.

Molecule stacking and film morphology

Molecular packing style in film state is very important to the device performance. Therefore, tuning molecular structure is proved to be an effective way to achieve desired molecular packing style in solid state.^{7(b)} In our previous work, we successfully adjusted the molecular packing style and the intermolecular π - π stacking distance through the changing of molecular planarity. To verify the result in this work, X-ray diffraction (XRD) patterns of ID(BT)2 and ID(BF)2 based thin films were measured.

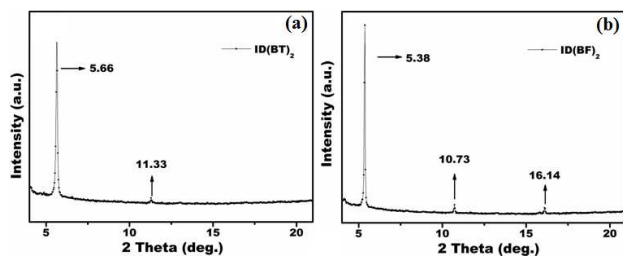


Fig. 3 The X-ray diffraction (XRD) patterns of ID(BT)2 and ID(BF)2. (a) ID(BT)2; (b) ID(BF)2

As shown in Fig. 3a, ID(BT)2 shows a sharp diffraction peak at 5.66° corresponding to a d -spacing of 15.6 Å which belongs to the long-range arrangement, and the second order diffraction peak at 11.33° is also observed which indicates a layer-by-layer stacking in film

state. For ID(BF)2, the diffraction peak located at 16.14° with the d -spacing of 5.48 Å is corresponding to the weak intramolecular π - π stacking which mainly due to the almost planar structure while that located at 5.38° with the d -spacing of 16.42 Å is consistent with the long-range stacking. Meanwhile, the second order peak is also found at 10.73° and the diffraction peak at 16.14° is recognized as the third order peak, which illustrates a more regular molecular stacking for ID(BF)2 in the film state and thus facilitates the charge transition throughout the films.

Atomic force microscopy (AFM) is also carried out to measure the molecular morphology from the surface (Fig. S3). The surface morphology of ID(BT)2 based film shows a network structure with the surface root-mean-square (RMS) roughness of about 5 nm. The relative large RMS is not beneficial for the charge transition through the films and will increase the energy barrier between the organic layers and the top Al electrodes. In contrast, due to the almost planar molecular backbone and the more ordered stacking in film state, the RMS of ID(BF)2 based film is measured to be as little as 1 nm. The smooth surface morphology facilitates the charge injection from the electrode into the active layers and is conducive to the transition of the charge carriers through the films. Thus, more power is needed to overcome the energy barrier and the threshold voltage of ID(BT)2 based memory device may be larger than that of ID(BF)2.

Memory Performance

The I - V characteristics of ID(BT)2-based device were measured and shown in Fig. 4a. When a negative bias was applied (0 to -3.5 V, Sweep 1), initially, the device was in the low conductivity (OFF) state. As the negative bias approached to -2.2 V, an abrupt increase in the current (10^{-8} A to 10^{-3} A) took place, indicating the transition from the low conductivity (OFF) state to the high conductance state (ON). This conductivity convert from OFF to ON state is referred to as a writing process. The device maintained in the high conductance state, as indicated by the subsequent Sweep 2 and 3. After turning off the power for a period of ca. 8 min, the memory device was found to relax to the initial OFF state. The memory device can be switched to the ON state once again with the 4th Sweep. These results indicate that the ID(BT)2-based device can be repeatedly written with negative threshold voltages. The volatile nature of the ON state suggests that the ID(BT)2-based device exhibits the SRAM type memory.

Fig. 4d shows the I - V electrical switching of the ID(BF)2-based memory devices. Initially, the device was in a low conductance state (OFF) during the voltage sweep from 0 to -3.5 V (-3.5 V, Sweep 1). When the voltage achieved approximately -1.9 V, the current increased abruptly from 10^{-8} A to 10^{-3} A, which corresponds to the on-switching from the low conductivity (OFF) state to the high conductivity (ON) state. The device can relax to the OFF state after

ca. 2 min and can be repeatedly switched on during the subsequent negative sweep (Sweep 2 and Sweep 3). The ID(BF)2-based memory devices showed a volatile nature and could be switched on again with a negative bias (0 to -3.5 V), which can be utilized as a DRAM device. Meantime, the threshold voltage of ID(BF)2 is smaller that of ID(BT)2, which is in consistent with the analysis in the XRD and AFM measurements.

The stability tests of ID(BT)2 and ID(BF)2 based memory devices were also evaluated at room temperature. Fig. 4b and 4e show that both devices are stable for about 600 s under a constant stress of -1V for both ON and OFF states, and no obvious degradation in current was observed during the periods of test. No resistance degradation was observed for the ON and OFF states during 10^6 read cycles for both devices under continuous read pulses at -1 V on both ON and OFF states, as showed in Fig. 4c and 4f.

In order to exclude the possible metal filaments happened in memory behaviours, sandwich structured memory devices ITO/small molecules/LiF/Al were fabricated under the same condition. The LiF layer (5 nm) was served as a buffer layer to prevent the aluminium nanoparticles penetrating into the active films. The I - V results indicated the invariable memory behaviours for ID(BT)2 and ID(BF)2 based memory devices, as shown in Fig. S4, which demonstrated that the SRAM and DRAM memory behaviours were irrelevant to the metal filament.

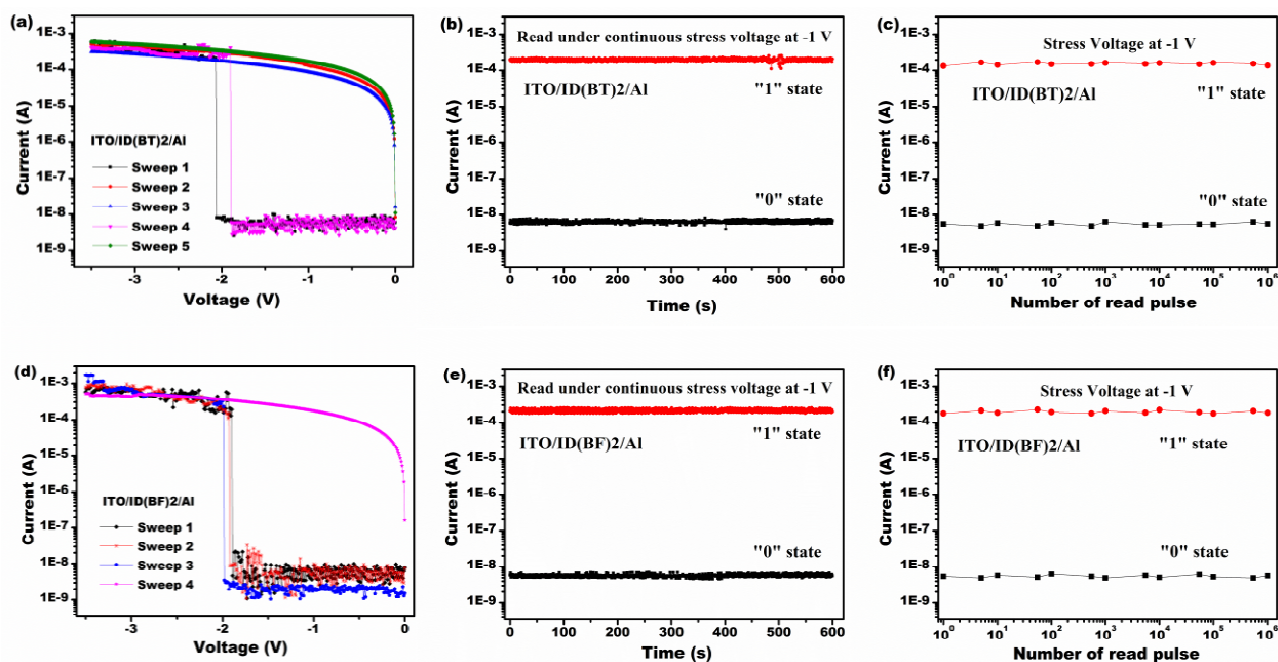


Fig. 4 Typical Current-Voltage (I - V) characteristics of the ID(BT)2 memory device (a), and ID(BF)2 memory device (d); stability test of the memory device in two states under a constant read voltage of -1 V, (b) ID(BT)2, (e) ID(BF)2; stimulus effect of read cycles on two states under continuous read pulses at -1 V, (c) ID(BT)2, (f) ID(BF)2

In order to understand the switching mechanisms of the memory devices, quantum chemical calculations were performed based on the DFT with the Gaussian 03 program (Fig. 5). The HOMOs are

distributed over the whole conjugated molecular backbone, whereas the LUMOs are mainly located on the isoindigo moieties. Due to the obvious asymmetric distribution of the HOMO and

LUMO energy levels, the charge transfer process can easily occur under an applied voltage.¹⁸ Charge transfer complexes can be formed during the electron transition from benzothiophene and benzofuran to isoindigo units, and the complexes can be decomposed when the external voltage was removed. Therefore, both devices are showing a repeatable volatile storage features.

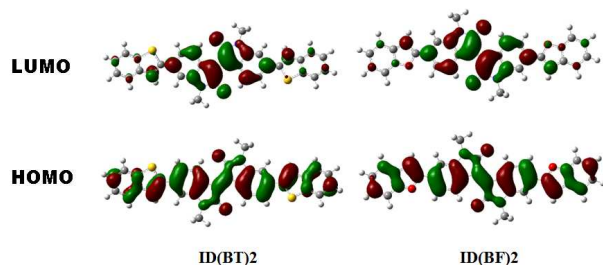


Fig. 5 The frontier molecule orbital (LUMO, HOMO, bottom) obtained from DFT calculations on the molecule.

To investigate the reason that ID(BT)2 and ID(BF)2 with different storage types, further analysis of the molecular geometry of ID(BT)2 and ID(BF)2 were optimized from the DFT calculations. As depicted in Scheme 1, the dihedral angle between ID and BF is 0.3° (ID(BF)2) while that between ID and BT is 23° (ID(BT)2). The smaller dihedral angle of ID(BF)2 was attributed to the smaller size of oxygen than that of sulfur.¹⁹ Furthermore, according to Gerge. M's plotted curves of intramolecular charge transfer rate vs. dihedral angle,²⁰ the charge transfer rate with 0° dihedral angle is almost 4 times faster than that with 23° dihedral angle, which is corresponding to the recovery time for ID(BF)2 of 2 minutes and for ID(BT)2 of 8 minutes. Meantime, the smaller dihedral angle caused the almost planar molecular backbone which was beneficial for the migration of the charge carriers and was advantageous to the transferred charges moving back to the initial donors. Subsequently, such different dihedral angles may have a big impact on the molecular stacking in film state which is the main factor to affect the performance of the devices. Compared to the twist molecule ID(BT)2 with a dihedral angle of 23° , the molecule ID(BF)2 with a dihedral angle of 0.3° formed a weak intramolecular π - π stacking in film state according to the XRD measurements, which illustrated more regular stacking in film state that facilitated the charge transition throughout the films and further the transferred charges moving back to the initial donors. In addition, the surface morphology of ID(BT)2 based film shows a network structure with the surface root-mean-square (RMS) roughness of about 5 nm. The relative large RMS is not beneficial for the charge transition through the films and will increase the energy barrier between the organic layers and the top Al electrodes. In contrast, due to the almost planar molecular backbone and the more ordered stacking in film state, the RMS of ID(BF)2 based film is measured to be as little as 1 nm. The smooth surface morphology facilitates the charge injection from the electrode into the active layers and is conducive to the transition of the charge carriers through the films, which is also advantageous to the process of the transferred charges moving back to the donors. Therefore, ID(BT)2 based device displays SRAM storage type, while ID(BF)2 based device presents DRAM storage type.

Conclusions

Two D-A-D structured molecules, ID(BT)2 and ID(BF)2, were designed and synthesized. ID(BF)2 showed a much smaller dihedral angle than that of ID(BT)2 according to the theoretical calculations due to the smaller atomic size of O, which is conducive to the migration of the charge carriers in the backbone. At the meantime, ID(BF)2 based film processed more ordered stacking in film state, which was beneficial for charge transition through the films and had a big impact on memory performance. The sandwich structured memory device of ID(BF)2 exhibited DRAM behaviours and that of ID(BT)2 showed SRAM characteristic, which could be explained by the different dihedral angles and molecular stacking and morphology. We envision the work will pave the way for future materials design for volatility memory device.

Acknowledgments

This work was financially supported by the NSF of China (21176164, 21206102, 21336005 and 21476152), the NSF of Jiangsu Province (BE2013052), a project supported by the Specialized Research Fund for the Doctoral Program of Higher Education of China (Grant No. 20123201120005), Chinese-Singapore Joint Project (2012DFG41900) and National Excellent Doctoral Dissertation funds (201455).

Author contributions

Haiyan Hu synthesized the molecules and was involved in electrical measurements. Jinghui He executed the simulation calculations. Erbo Shi and Hao Zhuang performed the XRD and the AFM experiments. Jianmei Lu and Hua Li were initially involved in molecular design and supervised the whole experiment. All authors contributed to the scientific discussion, writing and revision of the manuscript.

Notes and references

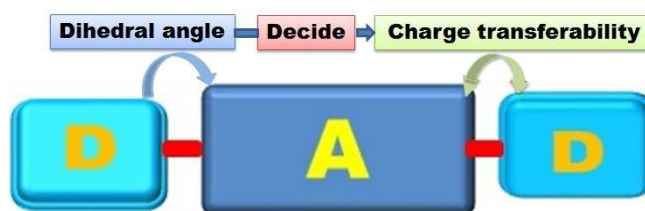
- (a) Y. C. Chiu, T. Y. Chen, Y. G. Chen, T. Satoh, T. Kakuchi, and W. C. Chen, *Appl. Mater. Interfaces*, 2014, **6**, 12780. (b) H. Li, Q. F. Xu, N. J. Li, R. Sun, J. F. Ge, J. M. Lu, H. W. Gu, F. Yan, *J. Am. Chem. Soc.*, 2010, **132**, 5542. (c) C. Y. Wang, J. X. Wang, P. Z. Li, J. K. Gao, S. Y. Tan, W. W. Xiong, B. L. Hu, P. S. Lee, Y. L. Zhao, Q. C. Zhang, *Chem. Asian. J.*, 2014, **9**, 779. (d) T. W. Kim, H. Choi, S. H. Oh, G. Wang, D. Y. Kim, H. Hwang, T. Lee, *Adv. Mater.*, 2009, **21**, 2497.
- (a) L. H. Xie, Q. D. Ling, X. Y. Hou, W. Huang, *J. Am. Chem. Soc.*, 2008, **130**, 2120. (b) H. Li, N. J. Li, R. Sun, H. W. Gu, J. F. Ge, J. M. Lu, Q. F. Xu, X. W. Xia, L. H. Wang, *J. Phys. Chem. C.*, 2011, **115**, 8288. (c) A. Stikeman, *Technol. Rev.*, 2002, **105**, 31.
- (a) Y. D. Lin and T. J. Chow, *J. Mater. Chem.*, 2011, **21**, 14907. (b) J. S. Lee, *J. Mater. Chem.*, 2011, **21**, 14097. (c) J. Liu, Z. Zeng, X. Cao, G. Lu, L. H. Wang, Q. L. Fan, W. Huang, H. Zhang, *Small*, 2012, **8**, 3517.
- (a) C. W. Chu, J. Ouyang, J. H. Tseng, Y. Yang, *Adv. Mater.*, 2005, **17**, 1440. (b) A. Bandyopadhyay, A. J. Pal, *Adv. Mater.*, 2003, **15**, 1949. (c) G. Li, K. Zheng, C. Y. Wang, K. S. Leck, F. Z. Hu, X. W. Sun, Q. C. Zhang, *ACS. Appl. Mater. Interfaces*, 2013, **5**, 6458.
- (a) Z. J. Liu, E. B. Shi, Y. Wan, N. J. Li, D. Y. Chen, Q. F. Xu, H. Li, J. M. Lu, K. Q. Zhang, L. H. Wang, *J. Mater. Chem. C.*, 2015, **3**, 2033. (b) H. Zhuang, Q. J. Zhang, Y. X. Zhu, X. F. Xu, H. F. Liu, N. J. Li, Q.

- F. Xu, H. Li, J. M. Lu, L. H. Wang, *J. Mater. Chem. C.*, 2013, **1**, 3816.
- 6 Miao, S.F.; Li, H.; Xu, Q.F.; Li, N.J.; Zheng, J.W.; Sun, R.; Lu, J.M.; Li, C.M. *J. Mater. Chem.*, 2012, **22**, 16582.
- 7 (a) Y. H. Zhang, H. Zhuang, Y. Yang, X. F. Xu, Q. Bao, N. J. Li, H. Li, Q. F. Xu, J. M. Lu, and L. H. Wang, *J. Phys. Chem. C.*, 2012, **116**, 22832. (b) S. F. Miao, H. Li, Q. F. Xu, Y. Y. Li, S. J. Ji, N. J. Li, L. H. Wang, J. W. Zheng, J. M. Lu, *Adv. Mater.*, 2012, **24**, 6210.
- 8 (a) J. H. Tsai, W. Y. Lee, W. C. Chen, C. Y. Yu, G. W. Hwang, and C. Ting, *Chem. Mater.*, 2010, **22**, 3290. (b) W. Y. Huang and C. D. Han, *Macromolecules*, 2012, **45**, 4425. (c) S. L. Lim, N. J. Li, J. M. Lu, Q. D. Ling, C. X. Zhu, E. T. Kang, and K. G. Neoh, *Appl. Mater. Interfaces*, 2009, **1**, 60. (d) W. Y. Lee, T. Kurosawa, S. T. Lin, T. Higashihara, M. Ueda, and W. C. Chen, *Chem. Mater.*, 2011, **23**, 4487.
- 9 G. Distefano, D. Jones, M. Guerra, L. Favaretto, A. Modelli, G. Mengoli, *J. Phys. Chem.*, 1991, **95**, 9746.
- 10 (a) T. Odajima, M. Ashizawa, Y. Konosu, H. Matsumoto and T. Mori, *J. Mater. Chem. C.*, 2014, **2**, 10455. (b) C. Mitsui, J. Soeda, K. Miwa, H. Tsuji, J. Takeya, and E. Nakamura, *J. Am. Chem. Soc.*, 2012, **134**, 5448.
- 11 (a) Y. Ren, A. M. Hiszpanski, L. s. Whittaker-Brooks, and Y. L. Loo, *Appl. Mater. Interfaces*, 2014, **6**, 14533. (b) A. Yassin, P. Leriche, M. Allain and J. Roncali, *New J. Chem.*, 2013, **37**, 502.
- 12 K. Oniwa, T. Kanagasekaran, T. Jin, M. Akhtaruzzaman, Y. Yamamoto, H. Tamura, I. Hamada, H. Shimotani, N. Asao, S. Ikeda, K. Tanigaki, *J. Mater. Chem. C*, 2013, **1**, 4163.
- 13 (a) W. Y. Lee, T. Kurosawa, S. T. Lin, T. Higashihara, M. Ueda and W. C. Chen, *Chem. Mater.*, 2011, **23**, 4487. (b) R. Schmidt, J. H. Oh, Y. S. Sun, M. Deppisch, A. M. Krause, K. Radacki, H. Braunschweig, M. Könemann, P. Erk, Z. N. Bao, and F. Würthner, *J. Am. Chem. Soc.*, 2009, **131**, 6215. (c) M. Gsänger, J. Hakoh, M. Könemann, H. W. Höffken, A.M. Krause, Z. N. Bao and F. Würthner, *Angew. Chem. Int. Ed.*, 2010, **49**, 740.
- 14 (a) H. Kim, H. W. Kim, C. Sakong, J. Namgoong, W. Park, M. J. Ko, C. H. Lee, W. I. Lee, J. P. Kim, *Org. Lett.*, Vol., 2011, **13**, 5784. (b) K. E. Horner, P. B. Karadakov, *J. Org. Chem.*, 2013, **78**, 8037. (c) L. Dou, J. Gao, E. Richard, J. B. You, C. C. Chen, K. C. Cha, Y. J. He, G. Li, Y. Yang, *J. Am. Chem. Soc.*, 2012, **134**, 10071. (d) Z. X. Cai, Y. L. Guo, S. F. Yang, Q. Peng, H. W. Luo, Z. T. Liu, G. X. Zhang, Y. Q. Liu, D. Q. Zhang, *Chem. Mater.*, 2013, **25**, 471. (e) X. C. Wang, Y. P. Sun, S. Chen, X. Guo, M. J. Zhang, X. Y. Li, Y. F. Li, H. Q. Wang, *Macromolecules*, 2012, **45**, 1208.
- 15 (a) M. Wang, X. W. Hu, P. Liu, W. Li, X. Gong, F. Huang, Y. Cao, *J. Am. Chem. Soc.*, 2011, **133**, 9638. (b)
- 16 (a) G. F. Tian, D. Z. Wu, S. L. Qi, Z. p. Wu, X. D. Wang, *Macromol. Rapid Commun.* 2011, **32**, 384. (b) Q. J. sun, H. Q. Wang, C. H. Yang, Y. F. Li, *J. Mater. Chem.*, 2003, **13**, 800.
- 17 Q. D. Ling, D. J. Liaw, E. Y. H. Teo, C. X. Zhu, D. S. H. Chan, E. T. Kang, K. G. Neoh, *Polymer*, 2007, **48**, 5182.
- 18 (a) K. L. Wang, Y. L. Liu, J. W. Lee, K. G. Neoh, and E. T. Kang, *Macromolecules*, 2010, **43**, 17. (b) Y. L. Liu, Q. D. Ling, E. T. Kang, K. G. Neoh, D. J. Liaw, K. L. Wang, W. T. Liou, C. X. Zhu and D. S. H. Chan, *J. Appl. Phys.*, 2009, **105**, 044501. (c) C. L. Liu, T. Kurosawa, A. D. Yu, T. Higashihara, M. Ueda and W. C. Chen, *J. Phys. Chem. C.*, 2011, **115**, 5930.
- 19 T. Umeyama, T. Takamatsu, N. Tezuka, Y. Matano, Y. Araki, T. Wada, O. Yoshikawa, T. Sagawa, S. Yoshikawa, and H. Imahori, *J. Phys. Chem. C.*, 2009, **113**, 10798.
- 20 A. Helms, D. Heiler, G. Mclendon, *J. Am. Chem. Soc.*, 1991, **113**, 4325.

Triggering DRAM/SRAM memory behaviors by single atom substitution to alter molecular planarity

Haiyan Hu, Jinghui He, Hao Zhuang, Erbo Shi, Hua Li*, Najun Li, Dongyun Chen, Qingfeng Xu, Jianmei Lu*, Lihua Wang

Table of Contents



Novelty: achieving different types of memory devices through single atom substitution to alter molecular planarity thus improve the intramolecular dihedral angle.